KSU Mühendislik Bilimleri Dergisi 28(1), 2025
Araştırma Makalesi

KSU J Eng Sci, 28(1), 2025
Research Article

Kahramanmaras Sutcu Imam University
Journal of Engineering Sciences

Geliş Tarihi : 06.09.2024
Kabul Tarihi :07.10.2024

Received Date : 06.09.2024
Accepted Date :07.10.2024

EVALUATION OF THE VESSEL WITH DIFFERENT STENOSIS STRUCTURES USING CFD APPROACH

FARKLI DARLIK YAPILARINA SAHİP DAMARIN HAD YAKLAŞIMI KULLANILARAK DEĞERLENDİRİLMESİ

Arif ÇUTAY [1*] (ORCID: 0000-0002-0057-9417)
Özdeş ÇERMİK[1] (ORCID: 0000-0001-9308-4589)
Ahmet KAYA[1](ORCID: 0000-0001-9197-3542)

[1] Kahramanmaraş Sütçü İmam University, Department of Mechanical Engineering, Kahramanmaraş, Türkiye

*Sorumlu Yazar / Corresponding Author: Arif ÇUTAY, arif.cutay@gmail.com

ABSTRACT

Stenosis of blood vessels is a common cardiovascular issue, and numerical simulation provides an accessible alternative to experimental studies. This study utilizes computational fluid dynamics (CFD) to simulate blood flow dynamics in stenotic vessels with varying dimensions and viscosity models, offering insights into how blood behaves under different conditions. Validation, conducted by comparing results with experimental data in the post-stenotic region, shows acceptable differences. Nine stenosis models were analyzed by altering stenosis length (from 13.75 mm to 27.5 mm) and height (from 2.2 mm to 4.4 mm) while testing three viscosity models: Newtonian, Power Law, and Carreau Law. Key variables such as wall shear stress (WSS), pressure drop, and maximum throat velocity were determined, and recirculation zones and streamline contours were observed. The results indicate that small changes in stenosis dimensions significantly impact flow dynamics. While Newtonian and Power Law models produce similar outcomes, different viscosity models alter flow results. Carreau Law shows maximum WSS values between 25 Pa and 125 Pa, compared to 1.5 to 10 Pa for the Newtonian and Power Law models under the same conditions.

Key Words: Blood flow dynamics, computational fluid dynamics, CFD non-Newtonian flow, wall shear stress, stenosis

ÖZET

Kan damarlarındaki stenoz, yaygın bir kardiyovasküler sorundur ve sayısal simülasyon, deneysel çalışmalara karşı erişilebilir bir alternatif sunar. Bu çalışma, hesaplamalı akışkanlar dinamiği (HAD) kullanarak farklı boyutlara ve viskozite modellerine sahip stenozlu damarlardaki kan akış dinamiklerini simüle etmektedir ve bu, kanın farklı koşullar altında nasıl davrandığına dair önemli bilgiler sağlamaktadır. Stenoz sonrası bölgedeki deneysel verilerle yapılan karşılaştırmalar sonucunda doğrulama, kabul edilebilir farklılıklar göstermektedir. Stenoz uzunluğu (13.75 mm'den 27.5 mm'ye) ve yüksekliği (2.2 mm'den 4.4 mm'ye) değiştirilerek dokuz farklı stenoz modeli analiz edilmiş ve üç viskozite modeli (Newtonian, Power Law, Carreau Yasası) test edilmiştir. Temel değişkenler olan duvar kayma gerilimi (WSS), basınç düşüşü ve maksimum boğaz hızı belirlendi ve resirkülasyon bölgeleri ile akım çizgileri konturları gözlemlendi. Sonuçlar, stenoz boyutlarındaki küçük değişikliklerin akış dinamiklerini önemli ölçüde etkilediğini göstermektedir. Newtonian ve Power Law modelleri benzer sonuçlar üretirken, farklı viskozite modelleri akış sonuçlarını değiştirmektedir. Carreau Law Modeli, maksimum WSS değerlerini 25 Pa ile 125 Pa arasında gösterirken, Newtonian ve Power Law modelleri aynı koşullar altında 1.5 ile 10 Pa arasında değerler göstermektedir.

Anahtar Kelimeler: Kan akış dinamikleri, hesaplamalı akışkanlar dinamiği, HAD, Newtoniyen olmayan akış, duvar kayma gerilimi, stenoz

INTRODUCTION

ToCite: ÇUTAY, A., ÇERMİK, Ö., KAYA, A. (2025). EVALUATION OF THE VESSEL WITH DIFFERENT STENOSIS STRUCTURES USING CFD APPROACH. *Kahramanmaraş Sütçü İmam Üniversitesi Mühendislik Bilimleri Dergisi, 28(1),* 245-257.

The blood vessel is one of the fundamental components of the cardiovascular system, along with the heart and blood. The occlusion of a blood vessel, called “stenosis,” distorts this system, which is a frequent medical issue. It can become a life-threatening condition when the occlusion rate exceeds the cardiovascular system's tolerance. Computational fluid dynamics (CFD) has a broad range of applications, including hemodynamic flows. CFD can provide a powerful contribution to estimating stenosis severity by giving insights into the flow properties of the narrowed vascular area. It is well known that CFD has been utilized by several researchers for simulating blood flow to aid in diagnosing and treating vascular problems. Many studies state that local hemodynamic results can assist in assessing the degree of stenosis (Zarins et al., 1983; Davies et al., 1986; Shaaban and Duerinckx, 2000). Wall shear stress (WSS) is closely related to the assessment of local hemodynamics due to the nature of fluid dynamics. While regions with low shear stress contribute to the formation and progression of stenosis, due to the increased residence time of lipid particles (Malek et al., 1999; Soulis et al., 2006), high WSS is associated with a higher risk of vascular wall rupture, platelet aggregation, or the progression of stenosis (Dolan et al., 2013; Kumar et al., 2021). The velocity profile of stenosis can be an effective tool for understanding the characteristics of stenosis. The recirculation zone in the post-stenotic region is inherently associated with severe stenosis and can also serve as a predictive parameter for the progression of stenosis. Additionally, increased or decreased velocity is a crucial measurement for evaluating the percentage occlusion of stenosis. The pressure drop is another flow dynamic property that is a decisive factor in maintaining flow without varying the flow rate. For this reason, heart function is strongly correlated with pressure drop, as the heart acts as a biological pump to deliver the necessary blood for the body's vital needs.

Numerous studies on hemodynamics utilize the CFD approach. Some of these studies are discussed in the following section. Razavi et al. numerically investigated different stenosis forms under pulsatile flow conditions using various viscosity models (Razavi et al., 2021). Their studies focused on 30-60% occlusion in symmetric stenosis in the carotid artery. It was shown that while viscosity models had similar trends, they differed in magnitude. They concluded that the narrowing of the blood flow area resulted in a larger recirculation zone and disturbed radial velocity profiles (Samady et al., 2011). Chan et al. conducted a numerical study on non-Newtonian blood flow in an axisymmetric stenosis model. They included elastic wall boundary conditions using the fluid-structure interaction module of ANSYS. The Power Law and Carreau non-Newtonian models were used to define blood rheology. It was reported that the Carreau model showed greater stress values compared to the Power Law model. Their results indicated that the elastic wall boundary condition had an insignificant effect on the flow results (Chan et al., 2005). Kumar et al. modeled non-Newtonian blood flow through successive stenoses under pulsatile flow conditions. Two stenosis occlusion rates were used, ranging from 20-80% compression. While their wall boundary condition was rigid, a sinusoidal velocity profile was applied as the pulsatile flow condition at the inlet. They demonstrated that the compression rate was directly proportional to the shear stress rate in the narrowing region for both cases (Kumar et al., 2021). Basavaraja et al. analyzed the WSS and the oscillatory shear index (OSI) distribution at different severities of stenosis in the carotid artery. Multiple CT volumes were used to obtain flow volumes for simulation, and stenosis occlusion rates ranging from 50-99% were measured using CT angiography (Basavaraja et al., 2017). Zun et al. studied the prediction of restenosis in stented geometry by simulating local coronary blood flow. They concluded that small vessel size was an independent risk factor for restenosis in stented vessels (Zun et al., 2021). Foong et al. simulated blood flow behavior in terms of stenosis and artery radius. Blood flow was assigned a uniform velocity profile at the inlet, with a rigid wall condition, and the flow was laminar and steady state. Four different radii and five different stenosis angles were used to compare cases. As a result of this simulation, maximum shear stress values were observed at the minimum radius, while shear stress increased with a larger stenosis angle (Foong et al., 2020). Lopes et al. examined the fluid-structure interaction in carotid blood flow to compare viscosity models. The Newtonian and Carreau viscosity models were used as rheological models in their study. The Womersley flow condition was chosen for the inlet boundary. It was shown that vascular wall displacement was not dependent on blood viscosity. However, it was observed that the Carreau viscosity model produced dramatically higher WSS values (Lopes et al., 2020). Rostami et al. compared the cases of anemic, normal, and hypertensive patients using the Carreau viscosity model in a bypass vein. Blood flow was assumed to have a uniform velocity profile at the inlet. It was shown that hypertensive patients had the highest WSS values at three different sections compared to others. From their simulation results, they concluded that the graft position is critical for the success of bypass surgery, as the point between the host and grafted vessel exhibited the maximum stress (Rostami et al., 2020). Zhao et al. investigated the efficacy of shunt operations for inferior vena cava stenosis using the CFD approach. The wall was modeled with a rigid boundary condition, and pressure was applied at the inlet. Distinctive results were observed pre- and post-operatively in terms of velocity, pressure, and WSS. They demonstrated the validity of CFD analysis for clinical use in monitoring the efficacy of vascular operations (Zhao et al., 2021). Elhanafy et al. computationally investigated the effect of changes in hematocrit levels on blood flow under different degrees of stenosis occlusion. The Newtonian

viscosity model was used for blood, and the vessel model had a diameter of 7 mm. Non-pulsatile flow conditions were applied at the inlet, and the vessel wall was assumed to be rigid. WSS, shear rate, pressure, and velocity were examined to illustrate variations between cases (Elhanafy et al., 2020). Abugattas et al. performed a numerical study on bifurcated vessel geometry using three different non-Newtonian viscosity models. They analyzed the bifurcation angle and 60% stenosis categorically. The study's results were examined in terms of WSS values under the Power Law, Carreau-Yasuda, and Cross viscosity models (Abugattas et al., 2020).

In summary, blood flow simulation has significant potential for defining flow disturbances based on the existing literature. This study aims to simulate blood flow reactions computationally by creating different stenosis dimensions. The stenosis models are designed proportionally to observe the effects of stenosis length and height. Additionally, different viscosity models are adopted in the blood flow simulation to evaluate the response to varying stenosis models.

MATERIAL AND METHOD

In the present work, a laminar, incompressible, and steady 3-D stenosis geometry is utilized. The geometry of the validation model is shown in Figure 1(a), consisting of a cylindrical tube with a diameter of 6 mm and a length of 216 mm. The stenosis has a 2.75 mm occlusion and a length of 21 mm. This validation geometry is directly adapted from the study (Ai et al., 2010). The geometry used in our numerical study is shown in Figure 1(b). The validation geometry features sharper edges compared to the geometry in the present study. Therefore, the geometry in this study has been modified to visualize the effects of stenosis height and length. Nine different stenosis geometries were created with varying stenosis heights and lengths to observe the flow dynamics, as illustrated in Table 1. The stenosis length was kept constant while the heights varied, and vice versa. This approach allows both effects to be examined numerically without influencing each other.

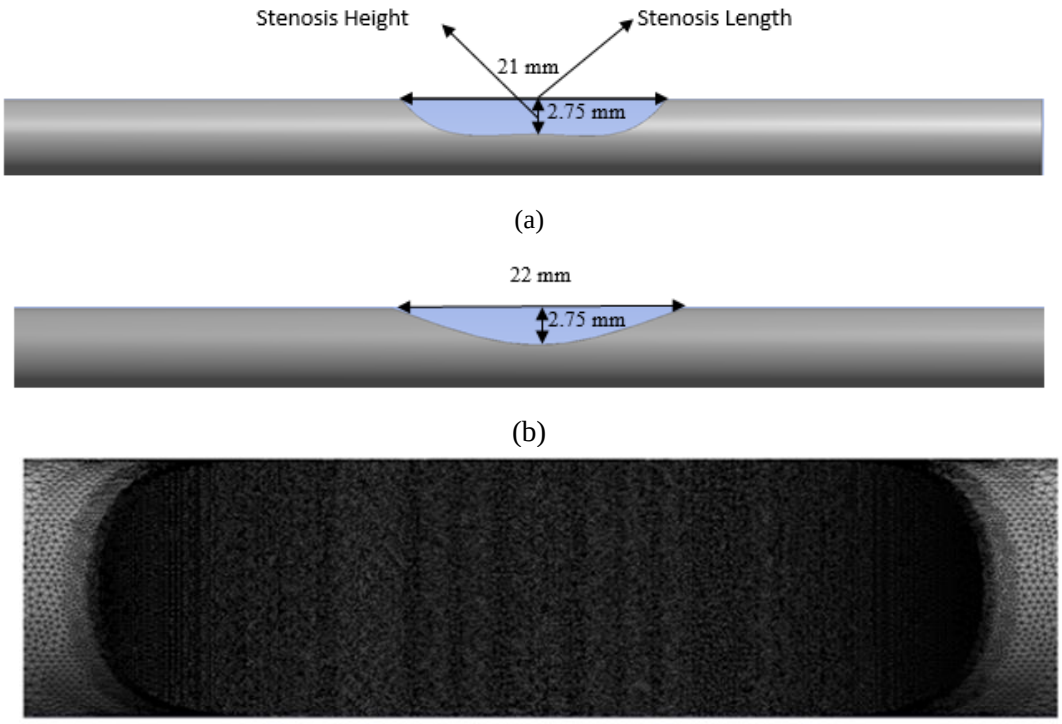

Figure 1. Illustration of Utilized Geometries and Mesh. (a)Validation Geometry (b) Geometry of Present Study (c) Mesh of Stenosis Region

The blood viscosity exhibits non-Newtonian characteristics due to the presence of red blood cells forming a suspension. However, many previous studies have considered blood as a Newtonian fluid (Basavaraja et al., 2017 ; Zun et al., 2021). Blood can only be approximated as Newtonian in larger arteries where the shear rate exceeds 100 s^{-1} (Samad et al., 2017). In this study, three different viscosity models—Newtonian, Power Law, and Carreau have been selected from the literature for comparison (Cho et al., 1991). Blood density is chosen as 1060 kg/m^3 (Hoskins

et al., 1990), and in the Newtonian model, blood viscosity is set at 0.00345 Pa·s. The non-Newtonian Carreau model used is shown below:

$$\mu = \mu_\infty + (\mu_0 - \mu_\infty)[1 + (\lambda\dot{\gamma})^2]^{(n-1)/2} \quad (1)$$

where time is constant $\lambda = 3.313$ s, zero strain viscosity is $\mu_0 = 0.056\ Pa.s$, infinite strain viscosity is $\mu_\infty = 0.00345\ Pa.s$, empirical exponent is $n = 0.3568$; and the Power Law model is shown as;

$$\mu = \mu_0(\dot{\gamma})^{n-1} \quad (2)$$

In the Carreau model, the nominal viscosity is set to μ_0 = 0.35 Pa·s, and the empirical exponent is n = 0.6. The governing equations are solved numerically under steady flow conditions using finite volume methods within ANSYS FLUENT. A second-order upwind scheme is used to discretize the Navier-Stokes equations for each control volume in the solution method section. Pressure-velocity coupling is achieved using the SIMPLE algorithm. A second-order upwind scheme is also applied for pressure interpolation, and least-squares cell-based methods are employed for spatial discretization. The simulation is considered converged when the residuals for all equations fall below 10^{-6} to ensure accuracy in comparison with experimental data. The simulations are performed on a personal computer equipped with an Intel i7-6700HQ processor, 16 GB of RAM, and a 64-bit Windows 7 operating system.

Table 1. Characteristics of Stenosis Models

Models	Stenosis Dimension Ratio (SDR)	Length (L)	Height (H)	Reduction Rate (%)	Mesh Number	Maximum Skewness	Minimum Orthogonal Quality
Model 1	5	13.75	2.75	46 %	1.300.749	0.58	0.42
Model 2	6	16.5	2.75	46 %	1.297.809	0.58	0.42
Model 3	7	19.25	2.75	46 %	1.295.671	0.58	0.42
Model 4	8	22	2.75	46 %	1.293.918	0.58	0.42
Model 5	10	27.5	2.75	46 %	1.289.348	0.60	0.40
Model 6	5	22	4.4	73%	1.262.885	0.6	0.4
Model 7	6	22	3.67	61%	1.276.161	0.58	0.42
Model 8	7	22	3.142	52%	1.286.354	0.58	0.42
Model 9	10	22	2.2	37%	1.302.919	0.6	0.4

Validation of Numerical Study

The validation of the numerical results is confirmed against the corresponding experimental and numerical data of Ai et al., as seen in Figure 2, focusing on the post-stenotic region for axial velocity across the radial direction. The post-stenotic region is selected due to the presence of recirculation zones observed in the experimental study, making it suitable for validation. Our results show better agreement with the experimental data of Ai et al. at certain points compared to their numerical study. The discrepancies between the numerical and experimental studies are mainly concentrated near the wall region. These differences can be attributed to two main factors. From the experimental perspective, the nature of the ultrasound measurement technique using probes can disturb the flow field. Additionally, it is challenging to accurately measure flow close to the wall due to the effects of the wall on hydrodynamics. From a numerical perspective, modeling flow near the wall is difficult due to the rapid changes in flow characteristics within this boundary layer. Furthermore, detecting recirculation zones in small flow regions is highly sensitive to both modeling and resolution. Overall, our numerical study shows results within acceptable limits when compared with the experimental data.

Grid Independence

Mesh independency is achieved using 6 different mesh numbers. Finer mesh is utilized at the stenotic region to capture the velocity gradient in detail as shown in Figure 1 (c). The optimum mesh number has been chosen as 1.2 million to save computational effort. Increasing the mesh number above the optimum mesh number does not significantly affect the results of the present study as illustrated in Figure 3.

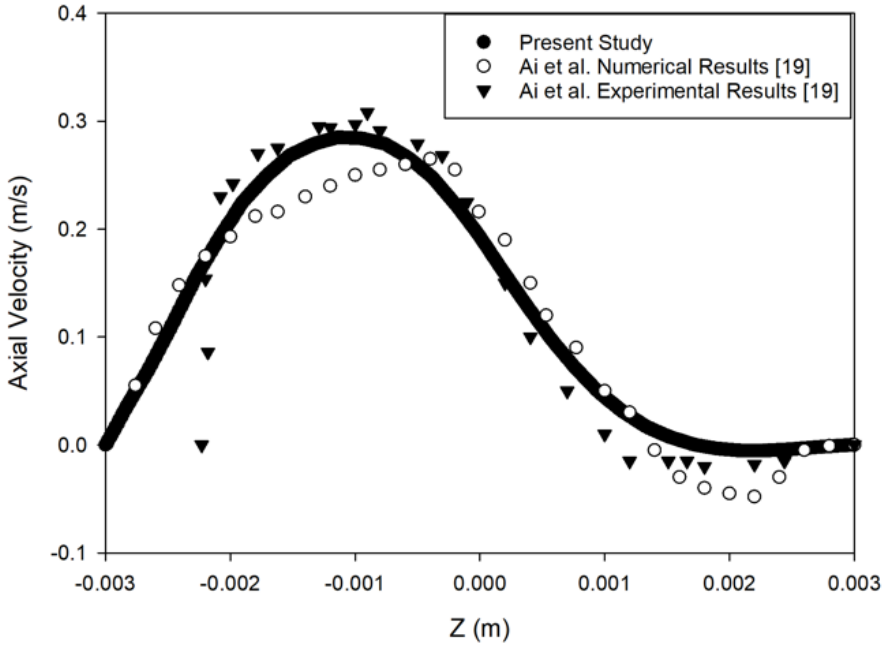

Figure 2. Validation of Numerical Results with Corresponding Experimental and Numerical Studies

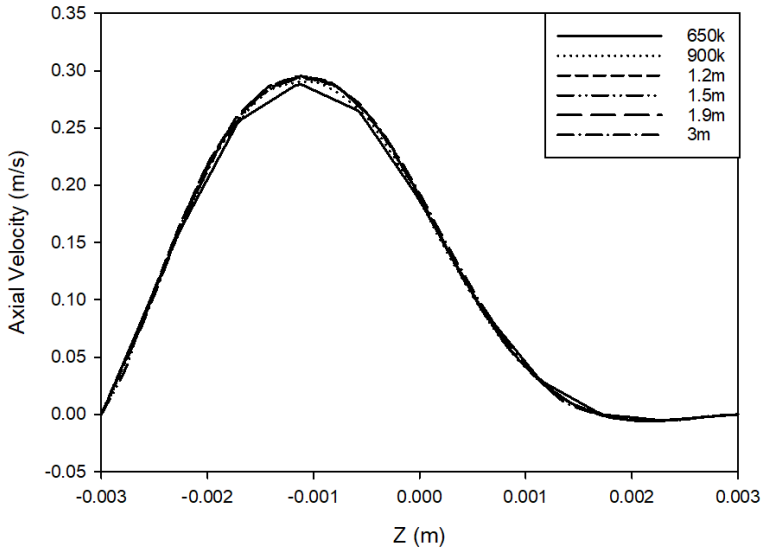

Figure 3. Mesh Independency Study

Boundary Condition

For this study, the non-pulsatile inlet boundary condition which is 0.00265 kg/s taken purely from experimental data (Chan et al., 2005; Elhanafy et al., 2020; Ai et al., 2010) is utilized. Rigid wall boundary condition is selected. Pressure outlet boundary condition is the outlet choice as atmospheric pressure.

RESULTS AND DISCUSSION

The blood flow properties in a stenotic vessel are quantified and visualized for different viscosity models through various flow dynamic parameters, including wall shear stress (WSS), pressure drop, velocity, detection of recirculation zones, and flow streamlines. The simulation of blood flow is conducted to investigate the effects of stenosis dimensions. In this chapter, the results of blood flow dynamics are presented, focusing on the WSS in the throat region, pressure drop across the stenosis, and maximum velocity values for three different viscosity models and nine different stenosis geometries. The simulations reveal distinctive results across the varying stenosis geometries.

Wall Shear Stress

The relationship between the initiation and development of stenosis and wall shear stress (WSS) has been studied extensively by researchers (Marshall et al., 2004; Pandey et al., 2020; Costa et al., 2016). WSS, defined as the dynamic force exerted by blood flow on the vessel wall, is a critical parameter in stenosis research. In this study, different stenosis models revealed varying WSS values, with the throat region consistently exhibiting significantly higher WSS compared to the pre- and post-stenotic regions across all viscosity models. The trends were similar across all viscosity models, though the WSS values differed, particularly at the throat. An exponential increase in WSS was observed as the stenosis dimension increased from Model 9 (2.2 mm) to Model 6 (4.4 mm). However, a sudden jump in WSS occurred between Model 6 (3.67 mm) and Model 7 (4.4 mm). The highest WSS was found at the narrowest height, while the largest stenosis height showed the lowest WSS, validating the use of WSS in assessing stenosis severity. Stenosis length had minimal impact on WSS in the throat and post-stenotic regions, but a slight increase in WSS was observed in the pre-stenotic region for longer stenosis models in the Newtonian and Power Law models. The Carreau model, however, showed a steady increase in WSS with increasing stenosis length for both pre- and post-stenotic regions. Among the viscosity models, the Newtonian and Power Law models exhibited the most distinctive WSS variations in the pre- and post-stenotic regions, while the Carreau model displayed similar characteristics across these regions but had notably higher WSS at the throat. This highlights the Carreau model's sensitivity in detecting differences between stenosis models at the throat. Comparatively, the WSS in the pre- and post-stenotic regions showed little variation across different viscosity models, and the stenosis length did not significantly affect WSS at the throat for models with constant stenosis height. However, pre-stenotic WSS increased consistently with stenosis length across all models. The throat WSS results for the Newtonian model were compared with Elhanafy et al.'s study, where maximum WSS ranged from 1 Pa to 24 Pa for various stenosis occlusion rates, while our study showed a range of 1.5 Pa to 10 Pa. The WSS results for Model 8, with a 52% occlusion rate, closely aligned with the 50% stenosis occlusion geometry in their study. Additionally, the Power Law model's WSS values ranged from 1.5 Pa to 10 Pa at the throat, showing an increasing trend similar to other studies as stenosis occlusion rates rose (Abuguttas et al., 2020). The Carreau model's WSS results, particularly for Model 9 with mild stenosis, were approximately 25 Pa, consistent with Chan et al.'s findings for similar throat region stenosis dimensions (Chan et al., 2005). Overall, these results demonstrate that WSS is a valuable metric for assessing stenosis severity, with sensitivity varying across different viscosity models.

Pressure Drop

Pressure drop is a fluid dynamic parameter that measures the loss of pressure between two points along the flow path, and it is directly related to the power consumption of systems, such as the heart in the circulatory system. Contraction or expansion of the flow area, as occurs in stenosis, is a common cause of pressure drop in blood flow. Figure 5 shows the pressure drop for different stenosis geometries, measured at pre- and post-stenosis points using three viscosity models. While the pressure drop trend follows a similar pattern to that of the wall shear stress (WSS), the effect of increasing stenosis length is more evident for pressure drop. This effect is most pronounced in the Carreau viscosity model compared to the other models. Despite this, the Carreau model shows the lowest overall pressure drop percentage, as it simulates lower viscous forces exerted on the blood flow. The Newtonian and Power Law models display similar trends, but the Newtonian model exhibits higher pressure drop percentages. Both the Newtonian and Power Law models indicate a greater pressure drop compared to the Carreau model. The narrowest stenosis geometry leads to the highest pressure drop, consistent with the WSS results. Conversely, the lowest pressure drop is observed in the longest stenosis length. Changes in stenosis height have a more noticeable effect on pressure drop than variations in stenosis length, indicating that a decrease in stenosis height poses a greater risk to heart function than an increase in stenosis length. Therefore, predicting pressure drop percentages can be an essential tool for estimating stenosis severity and assessing heart function in narrowing situations. Accurate modeling of stenosis geometry, based on medical imaging, is crucial for this process (Perinajová et al., 2021).

Velocity

Figure 6 illustrates the maximum velocity results for all stenosis models across three different viscosity models at the throat region. An increase in velocity in narrowed regions is expected according to the law of continuity.

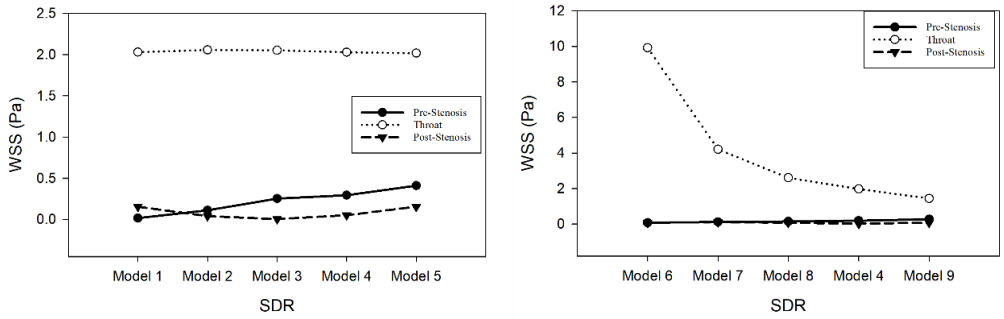

(a)

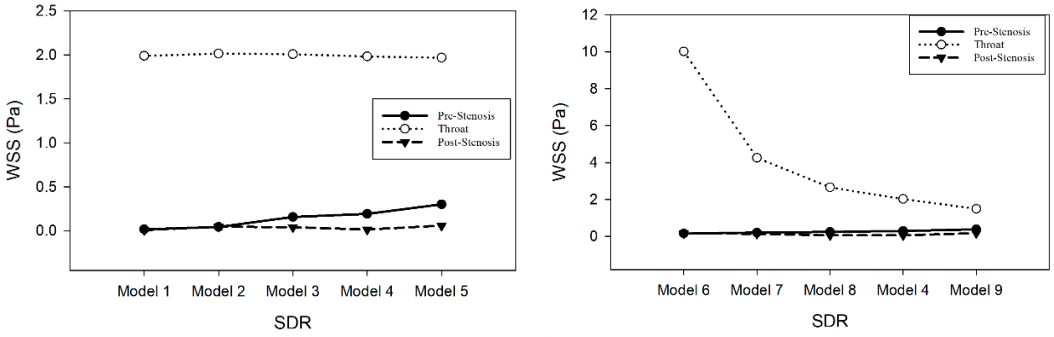

(b)

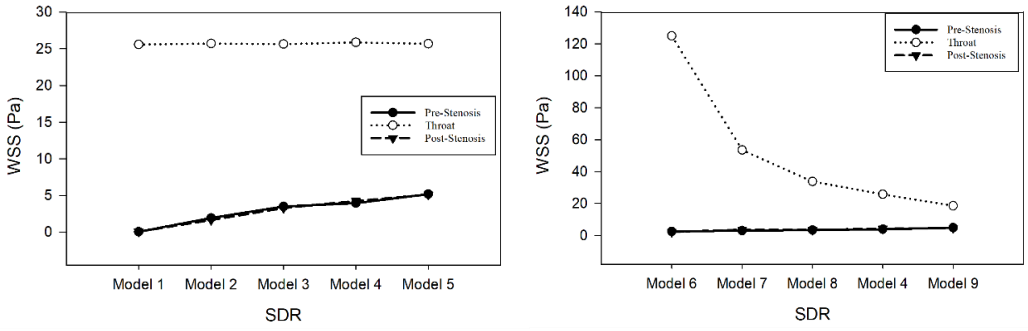

(c)

Figure 4. WSS Results of Nine Different Stenosis Geometries for Three Viscosity Models. Newtonian (b) Power Law (c) Carreau Law

However, it is important to observe how different viscosity models react to changes in stenosis height and length. Additionally, the maximum velocities at the pre- and post-stenotic regions provide valuable insights into blood flow dynamics in stenosis geometries. The narrowing of the region induces disturbances in flow both within and outside the stenosis. Numerical simulations are superior to experimental methods in obtaining sensitive measurements without disrupting the flow, as experimental measurements can be challenging due to the difficulty of placing probes accurately within the vessel. Stenosis length has a decreasing effect on blood velocity in the pre- and post-stenotic regions. However, the throat velocity is only minimally affected by changes in stenosis length. Conversely, the maximum velocity occurs at the minimum stenosis length for all viscosity models when the stenosis height is held constant. The Power Law and Newtonian viscosity models show similar trends, which align with the WSS results. The Carreau model, however, yields the highest velocities for both pre- and post-stenotic regions. Variations in stenosis dimensions not only increase throat velocity but also lead to higher velocities in the pre- and post-stenotic regions. Velocity of this study has congruence with respect to Samad et al. study in terms of magnitude change at pre and post stenotic regions for Newtonian model. However, In the non-Newtonian model, the velocity results have not

been higher, contrary to our study. This may be due to the different input of the subparameters of the non-Newtonian model, specifically the Carreau model (Samad et al., 2017).

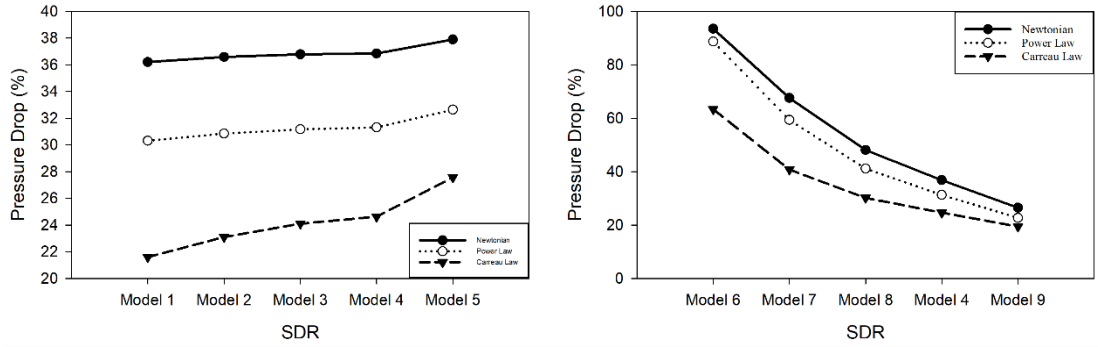

Figure 5. Pressure Drop of Different Stenosis Geometries between Pre- and Post-Stenosis Points for Three Viscosity Models.

Recirculation Zone

Recirculation zones are fluid dynamic phenomena indicating severe stenosis, described as the "reaction of fluid to a sudden change in flow area." This condition is significant in blood flow dynamics, as it can both classify the degree of vessel occlusion in terms of risk and serve as an indicator of clot formation and stenosis progression (Sharifzadeh et al., 2020; Gallo et al., 2014). Figure 7 presents vector plots of stenosis at the post-stenotic region, highlighting recirculation zones near the vessel wall for all viscosity models. In this study, recirculation zone characteristics are observed for the Newtonian and Power Law viscosity models in three cases: Model 6 (4.4 mm height), Model 7 (3.67 mm diameter), and Model 8 (3.142 mm height). Different viscosity models result in varying distributions of the recirculation zone at the same stenosis model. Figure 7 clearly shows a dramatic increase in the magnitude of the recirculation zone with rising stenosis height. Similarly, narrowing the blood flow area enlarges the recirculation zone, and the formation point of the recirculation zone extends longitudinally with increased stenosis height. Model 8 exhibits a prominent recirculation zone for the Newtonian viscosity case, while the Power Law model shows a less distinct recirculation zone confined to a small area near the wall. Compared to Models 6 and 7, Model 8 demonstrates incipient recirculation zone characteristics and represents a turning point with a 52.45% occlusion rate in the stenosis models. Although both the Newtonian and Power Law models reveal recirculation zones at the stenosis wall, the Newtonian model shows more visible and pronounced vector arrows. In contrast, the Carreau model fails to display any recirculation zone vectors for any stenosis models or flow regions, making it unsuitable for detecting recirculation zones as a stenosis flow characteristic. As observed in this study, while the Newtonian model in the literature provides a wider recirculation area, the non-Newtonian model has shown recirculation flows in a narrower region (Rostami et al., 2020; Samad et al., 2017; Cho et al., 1991).

Streamlines

Interaction between fluid and the vein in which it flows is characterized by selected viscosity law. Reaction of fluid can be observed in detail through streamlines against the vein wall. Flow separation is an important parameter that defines the characteristics of flow. It changes with viscosity and flow area. Figure 8 displays the streamline of blood flow for nine different stenosis models and three different viscosity models to observe the zone of flow separation. Streamlines of the Carreau model flow closer to the wall region than other models at the post-stenotic region. It is hard to observe flow separation by utilizing the Carreau model since the flow vector sticks to the vessel wall due to the nature of the Carreau Law as you can see in Figure 7. This characteristic is coherent with the recirculation zone results of the Carreau model. The Newtonian and Power model shows similar streamlines characteristics which are analogous to the results of other flow properties. The recirculation zone of flow at the post-stenotic region shows congruence with streamlines flow behavior for these models in terms of flow characteristics among vessel wall and blood. Arrangements of streamlines are made to observe flow behavior effectively. In the first row, a picture of different stenosis lengths is placed under the same height at the post-stenotic region. The position of flow separation occurs at an earlier distance when the stenosis length is decreased. Besides, the flow has streamlines close to the wall at higher stenosis lengths. In the second row, streamlines are classified with regard to increasing stenosis height for

illustration of the stenosis height effect. Higher stenosis height produces more spaces for flow separation at the wall region. Furthermore, an increment of stenosis height is associated with earlier flow separation.

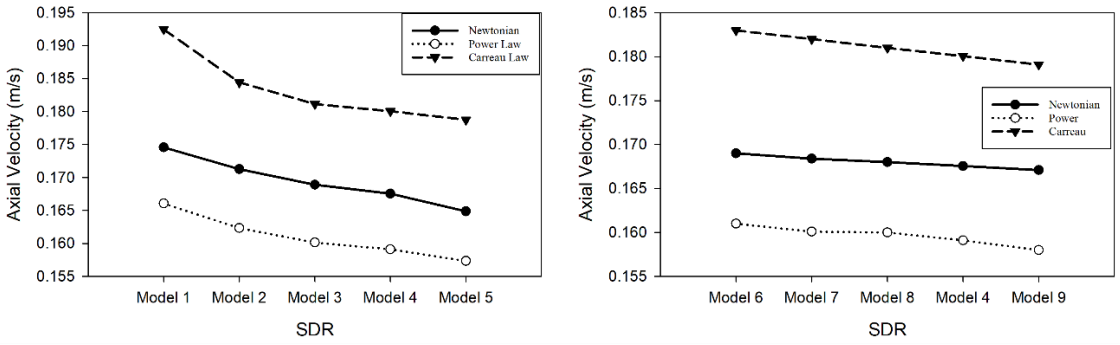

(a)

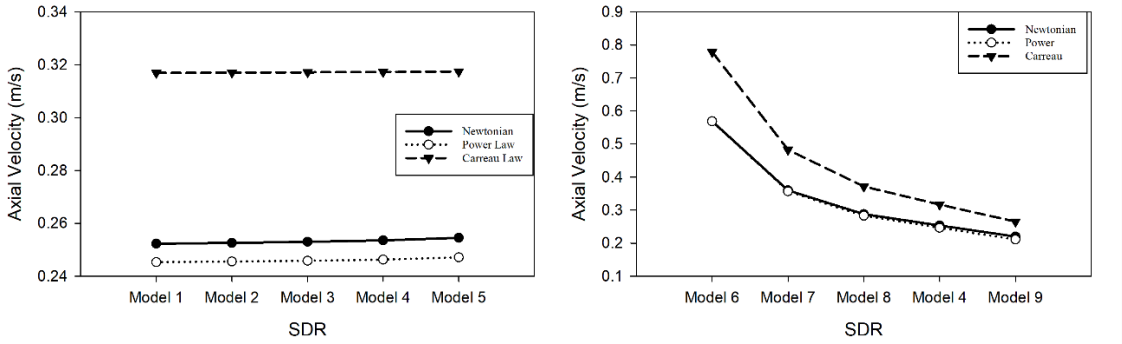

(b)

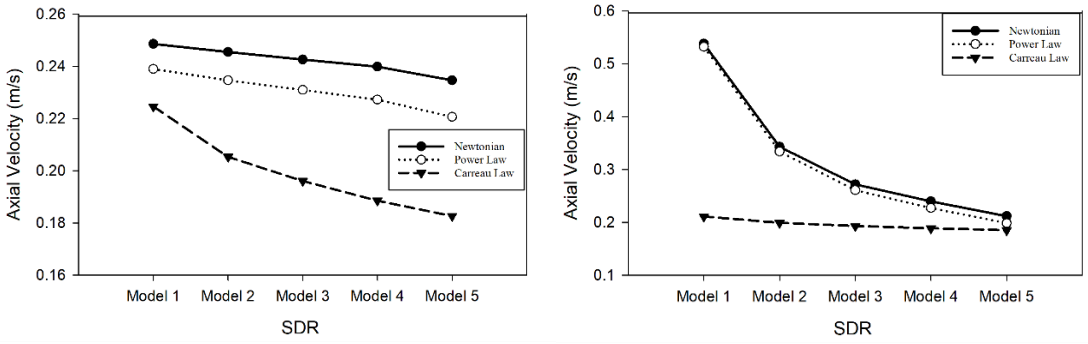

(c)

Figure 6. Maximum Velocity Values for Different Stenosis Geometries at Three Regions. Pre-Stenosis (b) Throat (c) Post-Stenosis

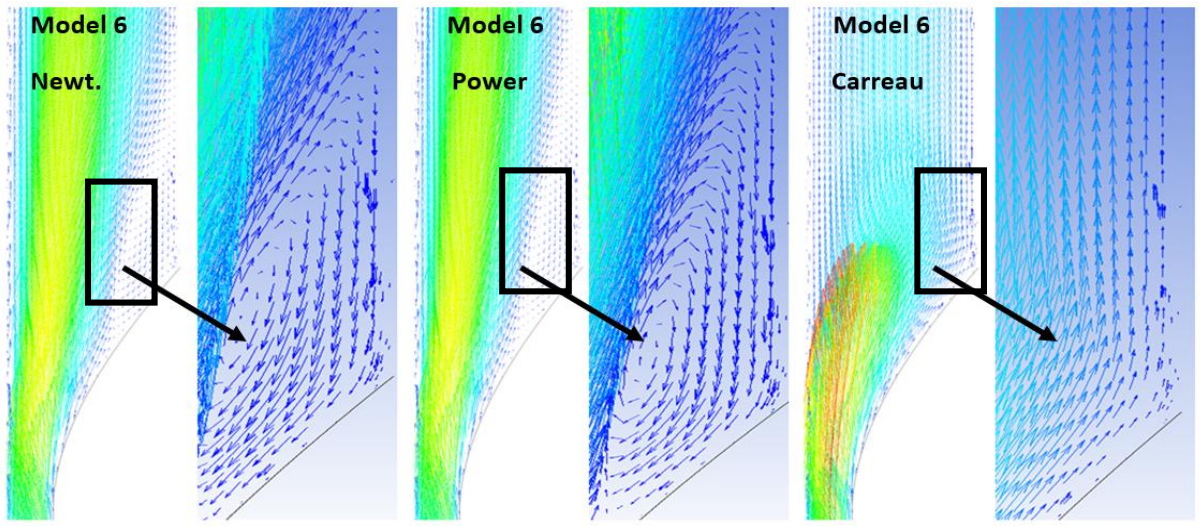

(a)

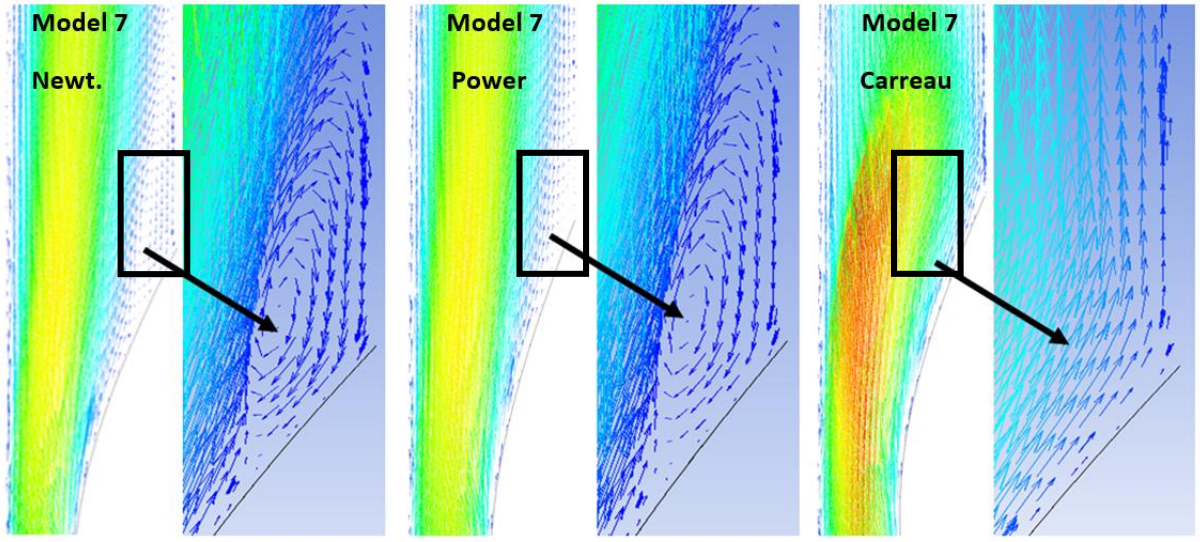

(b)

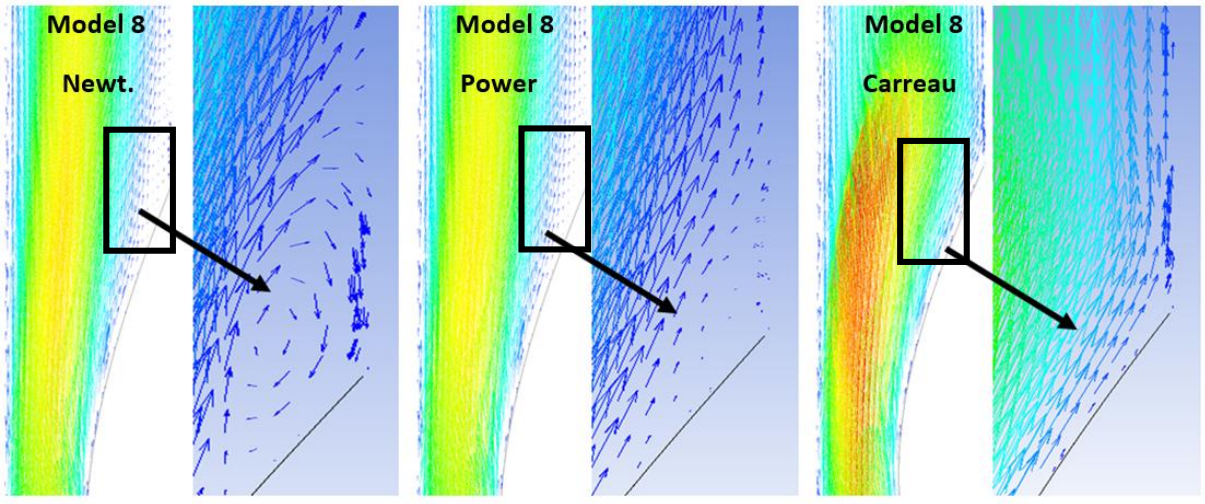

Figure 7. Velocity Vector Contours for Model 6 (a), Model 7 (b), and Model 8 (c) Post-Stenotic Region

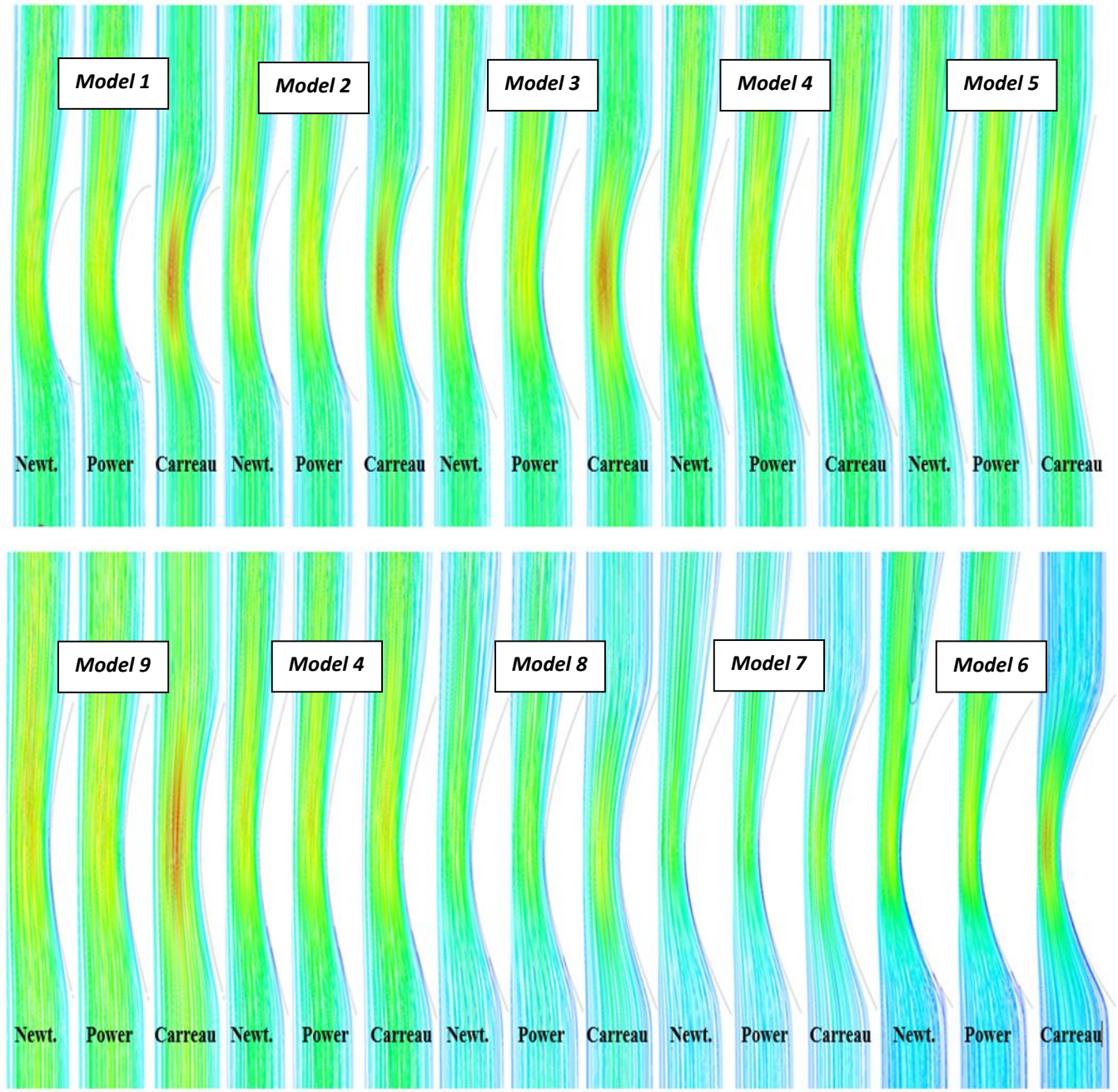

Figure 8. Streamlines of Nine Stenosis Models under Three Viscosity Models.

CONCLUSION

In this study, numerical simulations of nine different geometries are performed under three different viscosity models to observe the effect of both different geometries and viscosity models. Flow dynamic results are analyzed through the selection of appropriate parameters (WSS, pressure drop, velocities) with the help of open literature. Observation of flow characteristics is carried out with the help of analyzing streamlines and detecting recirculation zones. The following results are deduced in the consequences of numerical simulation by comparing different cases.

- The characteristic of the recirculation zone is seen only in four cases and two geometries at the post-stenotic region. These cases are the Model 6 and the Model 7 of the Newtonian and Power Law. The Carreau model cannot show any recirculation zone characteristic.
- The characteristic of flow separation is analyzed with the help of streamlines. Higher stenosis height and shorter stenosis length cause bigger flow separation areas at post-stenotic regions. The Carreau model is not convenient for observing flow separation while the Power and Newtonian give illustrations of flow separation.

- The WSS results show high rate of escalation at increasing height while stenosis length has a slight effect on the WSS results in the direction of rising.
- The stenosis height and length are highly correlated with pressure drop percentage. An increase in stenosis dimensions results in elevated pressure drop for all viscosity models. Pressure drop percentage results have been ordered in number as Newtonian>Power>Carreau with regard to viscosity models.
- The most affected area by the change in stenosis height is the throat area. At the same time, the stenosis model dimensions have a considerable effect on pre- and post-stenotic flow velocities. Therefore, pre- and post-stenosis regions should be taken into account for the correct examination of stenosis.
- The selected viscosity model has a significant impact on the sensitivity of the properties being studied. For this reason, the utilization of different viscosity models could be considered to obtain better sensitivity of viewed flow properties, especially for comparative studies.

REFERENCES

Abugattas, C., Aguirre, A., Castillo, E., & Cruchaga, M. (2020). Numerical study of bifurcation blood flows using three different non-Newtonian constitutive models. *Applied Mathematical Modelling*, 88, 529-549.

Ai, L., Zhang, L., Dai, W., Hu, C., Shung, K. K., & Hsiai, T. K. (2010). Real-time assessment of flow reversal in an eccentric arterial stenotic model. *Journal of Biomechanics*, 43(14), 2678-2683.

Basavaraja, P., Surendran, A., Gupta, A., Saba, L., Laird, J. R., Nicolaides, A., ... & Suri, J. S. (2017). Wall shear stress and oscillatory shear index distribution in carotid artery with varying degree of stenosis: a hemodynamic study. *Journal of Mechanics in Medicine and Biology*, 17(02), 1750037.

Chan, W. Y., Ding, Y., & Tu, J. Y. (2005). Modeling of non-Newtonian blood flow through a stenosed artery incorporating fluid-structure interaction. *Anziam Journal*, 47, C507-C523.

Cho, Y. I., & Kensey, K. R. (1991). Effects of the non-Newtonian viscosity of blood on flows in a diseased arterial vessel. Part 1: Steady flows. *Biorheology*, 28(3-4), 241-262.

Costa, E. D. (2016). Hemodynamics in the Left Coronary Artery-numerical and in vitro approaches (Doctoral dissertation, Universidade do Porto (Portugal)).

Davies, P. F., Remuzzi, A., Gordon, E. J., Dewey, C. F., & Gimbrone, M. A. (1986). Turbulent fluid shear stress induces vascular endothelial cell turnover in vitro. *Proceedings of the National Academy of Sciences*, 83(7), 2114-2117.

Dolan, J. M., Kolega, J., & Meng, H. (2013). High wall shear stress and spatial gradients in vascular pathology. Kumar, G., Kumar, H., Mandia, K., Zunaid, M., Ansari, N. A., & Husain, A. (2021). Non-Newtonian pulsatile flow through an artery with two stenosis. Materials Today: Proceedings.

Elhanafy, A., Elsaid, A., & Guaily, A. (2020). Numerical investigation of hematocrit variation effect on blood flow in an arterial segment with variable stenosis degree. *Journal of Molecular Liquids*, 313, 113550.

Foong, L. K., Shirani, N., Toghraie, D., Zarringhalam, M., & Afrand, M. (2020). Numerical simulation of blood flow inside an artery under applying constant heat flux using Newtonian and non-Newtonian approaches for biomedical engineering. *Computer Methods and Programs in Biomedicine*, 190, 105375.

Gallo, D., Gülan, U., Di Stefano, A., Ponzini, R., Lüthi, B., Holzner, M., & Morbiducci, U. (2014). Analysis of thoracic aorta hemodynamics using 3D particle tracking velocimetry and computational fluid dynamics. *Journal of Biomechanics*, 47(12), 3149-3155.

Hoskins, P. R., Loupas, T., & McDicken, W. N. (1990). A comparison of the Doppler spectra from human blood and artificial blood used in a flow phantom. *Ultrasound in Medicine & Biology*, 16(2), 141-147.

Kumar, G., Kumar, H., Mandia, K., Zunaid, M., Ansari, N. A., & Husain, A. (2021). Non-Newtonian pulsatile flow through an artery with two stenosis. Materials Today: Proceedings.

Lopes, D., Puga, H., Teixeira, J., & Lima, R. (2020). Blood flow simulations in patient-specific geometries of the carotid artery: a systematic review. *Journal of Biomechanics*, 110019.

Malek, A. M., Alper, S. L., & Izumo, S. (1999). Hemodynamic shear stress and its role in atherosclerosis. *Jama*, 282(21), 2035-2042.

Marshall, I., Zhao, S., Papathanasopoulou, P., Hoskins, P., & Xu, X. Y. (2004). MRI and CFD studies of pulsatile flow in healthy and stenosed carotid bifurcation models. *Journal of Biomechanics*, 37(5), 679-687.

Pandey, R., Kumar, M., & Srivastav, V. K. (2020). Numerical computation of blood hemodynamic through constricted human left coronary artery: Pulsatile simulations. *Computer Methods and Programs in Biomedicine*, 197, 105661.

Perinajová, R., Juffermans, J. F., Westenberg, J. J., van der Palen, R. L., van den Boogaard, P. J., Lamb, H. J., & Kenjereš, S. (2021). Geometrically induced wall shear stress variability in CFD-MRI coupled simulations of blood flow in the thoracic aortas. *Computers in Biology and Medicine*, 133, 104385.

Razavi, A., Shirani, E., & Sadeghi, M. R. (2011). Numerical simulation of blood pulsatile flow in a stenosed carotid artery using different rheological models. *Journal of Biomechanics*, 44(11), 2021-2030.

Rostami, S., Mozoun, M. A., Toghraie, D., Zarringhalam, M., & Goldanlou, A. S. (2020). Insight into the significance of blood flow inside stenosis coronary jointed with bypass vein: The case of anemic, normal, and hypertensive individuals. *Computer Methods and Programs in Biomedicine*, 196, 105560.

Samad, A., Husain, A., Zunaid, M., & Samad, A. (2017). Newtonian and Non-Newtonian Pulsatile Flows through an Artery with Stenosis. *The Journal of Engineering Research [TJER]*, 14(2), 191-205.

Samady, H., Eshtehardi, P., McDaniel, M. C., Suo, J., Dhawan, S. S., Maynard, C., ... & Giddens, D. P. (2011). Coronary artery wall shear stress is associated with progression and transformation of atherosclerotic plaque and arterial remodeling in patients with coronary artery disease. *Circulation*, 124(7), 779-788.

Shaaban, A. M., & Duerinckx, A. J. (2000). Wall shear stress and early atherosclerosis: a review. *American Journal of Roentgenology*, 174(6), 1657-1665.

Sharifzadeh, B., Kalbasi, R., Jahangiri, M., Toghraie, D., & Karimipour, A. (2020). Computer modeling of pulsatile blood flow in elastic artery using a software program for application in biomedical engineering. *Computer Methods and Programs in Biomedicine*, 192, 105442.

Soulis, J. V., Giannoglou, G. D., Chatzizisis, Y. S., Farmakis, T. M., Giannakoulas, G. A., Parcharidis, G. E., & Louridas, G. E. (2006). Spatial and phasic oscillation of non-Newtonian wall shear stress in human left coronary artery bifurcation: an insight to atherogenesis. *Coronary Artery Disease*, 17(4), 351-358.

Zarins, C. K., Giddens, D. P., Bharadvaj, B. K., Sottiurai, V. S., Mabon, R. F., & Glagov, S. (1983). Carotid bifurcation atherosclerosis. Quantitative correlation of plaque localization with flow velocity profiles and wall shear stress. *Circulation Research*, 53(4), 502-514.

Zhao, Y., Ping, J., Yu, X., Cui, Y., Yin, J., Sun, C., ... & Tang, L. (2021). Computational fluid dynamics simulation of time-resolved blood flow in Budd-Chiari syndrome with inferior vena cava stenosis and its implication for postoperative efficacy assessment. *Clinical Biomechanics*, 82, 105256.

Zun, P., Svitenkov, A., & Hoekstra, A. (2021). Effects of local coronary blood flow dynamics on the predictions of a model of in-stent restenosis. *Journal of Biomechanics*, 120, 110361.